JOURNAL OF MATERIALS SCIENCE 12 (1977) 2310–2328

Structure and properties of Nylon 6 and PET fibres: the effects of crystallite dimensions

D. C. PREVORSEK, Y. D. KWON, R. K. SHARMA
Chemical Research Center, Allied Chemical Corporation, Morristown, New Jersey 07960, USA

Analyses of mechanical and diffusive properties of fibres are described indicating strong lateral interactions between the microfibrils. These results show that uniaxially oriented polymers must be analysed in terms of a model where the crystallites are imbedded in an "amorphous" matrix. The equations are derived for modulus, strength and coefficient of diffusion in terms of crystallite dimensions, and the results compared with the experimental data. These results contradict the predictions of the microfibrils model where the properties are independent of the crystallite dimensions but depend solely on the degree of crystallinity.

1. Introduction

The structure of fibres is very complex and is the subject of numerous studies. It is well known that by varying the processing conditions and after-treatments it is possible to achieve technologically important variations in mechanical and diffusive properties. Many studies have been therefore carried out to establish correlations between these properties and morphological characteristics of fibres. A particularly promising and frequently suggested correlation involves the relationships between amorphous orientation functions and fibre modulus, strength and coefficient of diffusion. In attempts to use these relationships as a non-destructive fibre quality control we frequently observed significant deviations from the expected trends. The morphological analysis of these exceptional cases revealed that it is necessary to revise our present concepts of fibre structure.

In all cases investigated to date, we found that a structural model consisting of crystallites embedded in an amorphous matrix yielded better results than a microfibrillar model assuming relatively poor lateral interactions between the microfibril. The most important consequence of this is that the fibre properties do not depend only on the degree of crystallinity but also on the dimensions and spacings between the crystallites.

Small-angle X-ray diffraction and diffusion studies showed that the interfibrillar domains play an important role for the mechanical properties in fibres, while the microfibrils provide primarily the dimensional stability at elevated temperatures. Based on these findings we proposed a structural model which combines the elements of the microfibrillar and paracrystalline fibre models. Recently we examined these fibres by transmission electron microscopy using thin cross-sections. These studies confirmed our conclusions regarding the structure of PET and Nylon 6 fibres. These findings also show that the models of fibre strength, modulus and diffusion must be revised to include the dimensions of crystallites. This conclusion is important because most of previous studies ignored this effect in qualitative analyses of fibre properties. Therefore, it was desirable to review our data related to this problem in one article. In addition to the summary of morphological and property analyses we also included in this paper the unpublished derivations and an analysis of fibre strength which is consistent with the new fibre model.

2. Morphological background

2.1. Microfibrils and intermicrofibrillar domains

The mechanism of drawing and the structure of oriented polymers has been the subject of numerous investigations [1–6]. While minor differences in views still exist, most authors agree that the melt-spun and drawn PE, PP, Nylon and PET fibres consist of at least three distinct phases: amorphous and crystalline domains of the microfibril, and the interfibrillar matter.

Almost all morphological studies of fibres show microfibrils as a well defined element structure whose width usually falls in the range between 60 to 200 Å. The most important methods for studying the structure of microfibrils are electron microscopy and small-angle X-ray scattering (SAXS). Since these two techniques lead to essentially the same lateral dimensions of the microfibrils, there seems to be little doubt at present that the microfibrils must be regarded as a separate element of fibre structure. Nevertheless, less than a decade ago several prominent authors supported the idea that these fibres should be regarded as a one-phase paracrystalline structure.

The existence of microfibrils is not restricted to textile fibres; they appear also in drawn single crystals, drawn single crystal mats, drawn spherulitic sheets, solution-grown shish kebab fibres, capillary melt extrudates, solid-state extrudates and interlamellar links. Keller proposed that the microfibril can be divided into two classes [7]. Class (1) comprises substances whose molecules had been actually synthesized in the chain-extended form, such as biological fibres, crystals formed by *in situ* polymerization and structures resulting from stress- and flow-induced crystallization. When the microfibrils of Class (1) are heated close to the melting point the dimensions of the sample remain essentially unchanged. Class (2) comprises products of solid-state and melt drawing, in which the original crystalline or amorphous structure is destroyed, and the chains are aligned in the direction of the orienting force. The fibrils of Class (2) can shrink drastically when heated close to the melting point. The degree of shrinkage approximately equals the extent of deformation during original orientation.

Non-flow shrinkage experiments of Prevorsek and Tobolsky with melt-spun fibres show that with Nylon 6 and PET fibres at least 50% of total contraction is observed below the melting point of the fibre. The remaining part of contraction takes place very close or slightly above the melting point [8]. Consequently, these fibres must be regarded according to Barham–Keller criterion as inhomogeneous. It will be shown below that at temperatures considerably below the melting point, the shrinkage of fibres is caused primarily by the contraction of highly extended interfibrillar tie molecules. In this process the longitudinal structure of the microfibrils remains essentially unchanged because the contraction proceeds via lateral displacements of the microfibrils, while the changes in their longitudinal dimensions are minimal. The extended-chain interfibrillar domains formed between intermediate and high draw-ratios belong to the Class (2). These domains are responsible for shrinkage occurring below the melting point of the fibre. The microfibrils, on the other hand, belong very likely to Class (1) because the complete contraction of the fibre is achieved only at, or very slightly above, the melting point. This would indicate that the microfibrils are products of stress-induced crystallization. This means that their crystalline domains consist of elongated molecules produced by elongational flow.

The microfibrils in Nylon and PET fibres consist of a sequence of crystalline and amorphous domains whose dimensions along the fibre axis are sufficiently regular to act as a microlattice whose characteristics can be investigated by small-angle X-ray scattering. An important characteristic of the microfibril is the very long period which represents the spacing between two adjacent crystallites in the microfibril. Dimensions of the microfibrils found in Nylon, PET, PP and PE fibres are listed in Table I. With regard to the structure of the microfibril, it should also be noted that the crystallite length along the microfibril axis is always about $\frac{2}{3}$ of the long period.

The elements of microfibrils listed in Table I are the only characteristics of this structural unit whose dimensions are well defined. Not much work has been reported on the longitudinal dimensions of the microfibrils although some authors believe that the fracture of fibres under stress is

TABLE I Typical dimensions of the microfibrils (Å)

	PE	PP	Nylon	PET
Long period		90	90	150–180
Crystallite length		60	60	
Amorphous length		30	30	
Diameter	160	120–90		330–160

initiated at microfibril ends [9]. Recent studies of the structure of microfibrils by means of transmission electron microscopy from thin longitudinal sections of fibres indicated that the longitudinal dimensions of the microfibril are not well defined. Based on these studies, Reimschuessel and Prevorsek [10] conclude that the microfibrils form an essentially endless interwoven structure, where branching and fusion of microfibrils may be more characteristic than an abrupt end of the microfibril.

A great deal of work has been, heretofore, devoted to the structure of the microfibril; the nature and importance of the interfibrillar matter has attracted much less attention. First references to this matter appear in diffusion and deformation studies of Peterlin [1]. This author concludes that at least some of the interfibrillar space is filled with highly extended interfibrillar tie molecules which are the main factor in fibre shrinkage in the temperature range below their melting point. This view is supported by the analyses of Prevorsek *et al.*, which indicate that with Nylon and PET fibres, the volume fraction of the extended interfibrillar tie molecules is so significant that they should be considered as a separate phase [6, 11]. More work is needed to establish quantitatively the amount of these extended chains in various fibres.

Differences in opinion exist also with regard to the interactions between the microfibrils. Many authors concerned with the mechanical properties of fibres assume that the interfibrillar interactions are very small and thus the properties of fibres can be visualized as the properties of a loosely packed ensemble of the microfibrils [12, 13]. As a result, the modulus of a fibre as function of the degree of crystallinity was calculated as the modulus of an isolated microfibril. It is possible that this microfibrillar model is applicable to some forms of polyethylene and polypropylene fibres. The results and discussion below will show that, with PET and nylon fibres, the interaction between the microfibrils is sufficiently high to lead to conditions in which the crystallite dimensions have an important role in fibre modulus. This shows that the microfibrillar model, according to which the modulus is dependent on degree of crystallinity only, cannot be applied to these fibres.

The analysis of fibre strength is still a subject of intensive investigations. Two theories exist which could not be farther apart: Peterlin reasoned that the fibre strength should be attributed primarily to the strength of the microfibrils while the interfibrillar domains did not contribute a great deal to fibre strength [9]. It must be pointed out that this author and his coworkers primarily studied the structure and properties of polyethylene and polypropylene fibres and that these conclusions probably hold well for these fibres.

With Nylon and PET fibres, on the other hand, the situation seems to be quite different. According to the analyses of Prevorsek *et al.* [6, 11] the extended-chain interfibrillar domains are the strongest element of fibre structure, and have an important effect on fibre strength. The increase in fibre strength on drawing is attributed to an increase in the volume fraction of the extended-chain molecules which are formed as a result of the relative displacement of the microfibrils. In this process the molecules from the surface of the microfibrils are sheared off and stretched.

According to this model, the main role of the microfibrils is to provide dimensional stability at elevated temperatures, rather than contributing significantly to fibre strength. Note that the melting point of the microfibrils is considerably above the softening point of the extended interfibrillar regions, whose order and density are intermediate between that of the crystalline and amorphous domains of the microfibril.

A transmission electron photomicrograph of a thin cross-section (not stained) of a PET fibre is shown in Fig. 1. The light (the less dense) areas correspond to the microfibrils. Structural models consistent with SAXS, electron microscopy and diffusion analyses are shown in Figs. 2 and 3. The

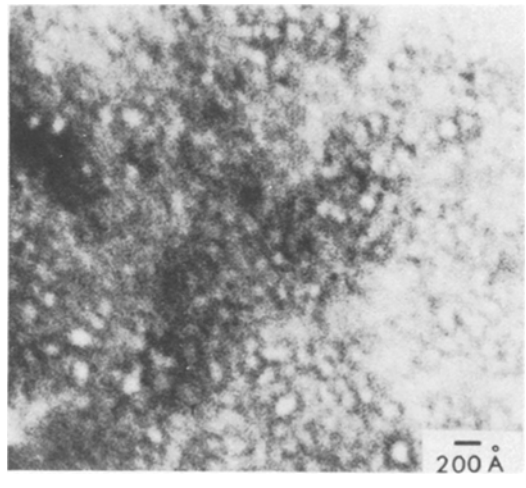

Figure 1 Transmission micrography of thin cross section in unstained sample of highly drawn PET fibre.

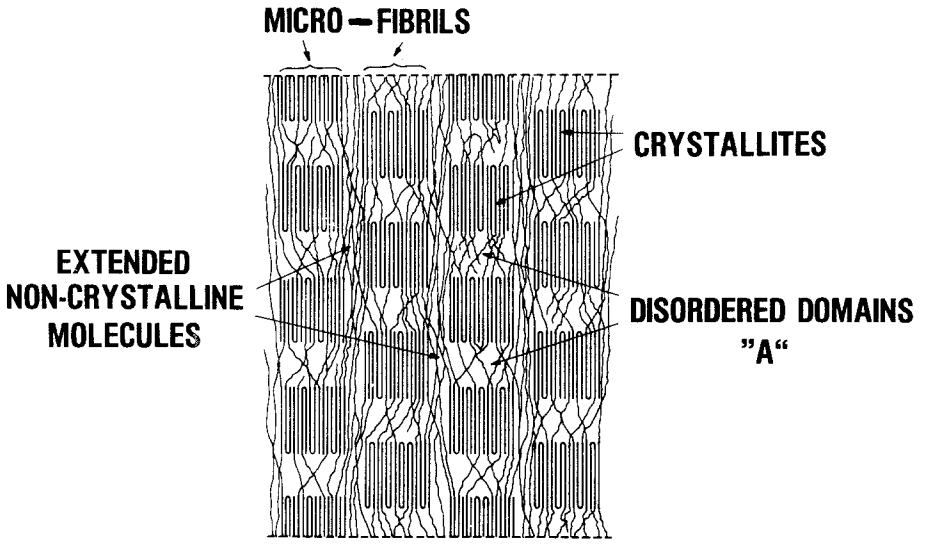

Figure 2 Schematic structure of PET fibres. Fibre axis vertical.

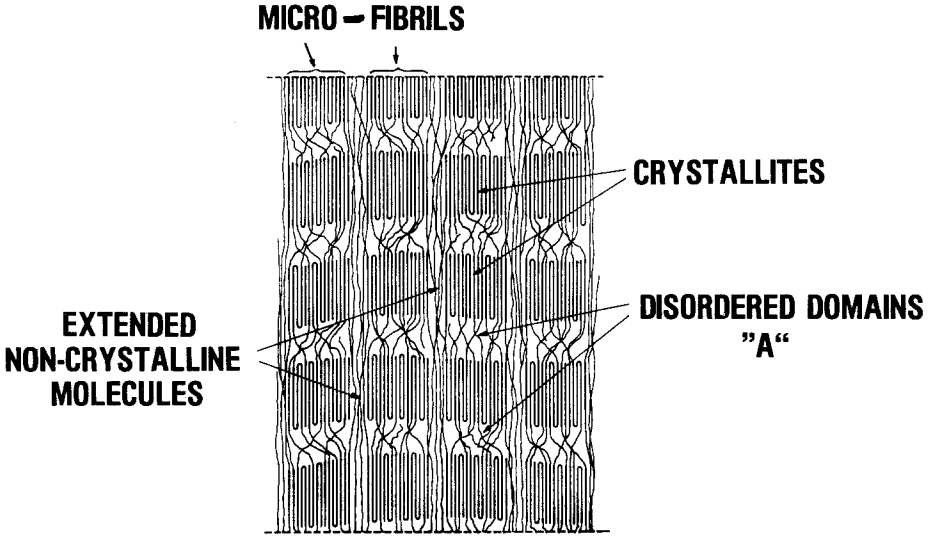

Figure 3 Schematic structure of Nylon 6 fibres. Fibre axis vertical.

arrangement of crystallites, staggered in PET and in layers with Nylon 6 is based on SAXS data for PET and SAXS and electron microscopy analyses for Nylon 6 [6, 10, 11].

2.2. Superfibrillar structure and fibrillation

An important characteristic of the model presented above is considerable interfibrillar strength, that is strength perpendicular to the fibre axis. Many fibres, including Nylon and PET, can be split easily in a direction parallel to the orientation. This tendency for splitting is so pronounced that it can be technologically exploited. There are many fibrillation processes in which oriented films or fibres are mecahnically split into fibres whose dimensions approach those of textile fibres [14]. Studies of Prevorsek *et al.* on fibre splitting showed that rolling, flexing, etc. of nylon fibres does not lead to splitting unless the fibres are spun with additives which form weak domains between nylon fibrils [14a]. On the basis of these results we implied that the interfibrillar strength of nylon fibres is considerable. In order to resolve this problem Reimschuessel and Prevorsek carried out a study of thin cross-sections from PET and Nylon fibres by means of transmission electron micro-

TABLE II Thickness of fibrils and interfibrillar regions in Nylon 6 fibres before and after staining with $SnCl_2$: effect of draw ratio

Draw ratio	Unstained		Stained	
	Thickness of fibrils (Å)	Thickness of interfibrillar regions (Å)	Thickness of fibrils (Å)	Thickness of interfibrillar regions (Å)
Undrawn	700–1000	700–1000	NI	NI
3 ×	NI	NI	500–600	500–600
5.35 ×	350–500	300–470	200–350	350–740

NI = Not investigated.

scopy [10] which supported the structural models presented in Figs. 2 and 3.

These studies revealed another element of fibre structure whose shape is ribbon-like and which has a thickness of about 300 to 400 Å in highly oriented Nylon 6, and is affected by fibre draw ratio. The $SnCl_2$ staining techniques and the details of sample preparation are discussed elsewhere [10]. The dimensions of these fibrils and interfibrillar region of Nylon 6 fibres before and after staining are summarized in Table II. A review of the literature data shows that this larger element of the structure was previously observed [15]. However, not enough attention has been paid to its dimensions and thus it was assumed that it is the microfibril. We propose that this element of the structure be referred to as the fibril because in many respects it bears a striking similarity with the microfibril. The fibrils can be readily resolved by ion-bombardment etching as shown by N. V. Hien *et al.* [15]. This treatment removes preferentially the less dense matter which separates the fibrils.

In longitudinal direction, the dimensions of the fibril are not well defined, because they form a branched and intertwined continuous network, similar to that of the microfibrils but on a larger scale. Near the surface, the fibrils are frequently oriented with their wider surface parallel to the fibre surface.

In the domains between the fibrils, one often observes longitudinal cracks which separate clusters of several hundreds of microfibrils. The tendency of fibres to split must, therefore, be attributed to the fibrillar structure of the fibre, and the existence of the cracks in the domains separating the fibrils [10]. Since the ease of fibre splitting can be controlled by varying the spinning and drawing conditions of fibre preparation, it appears that the nature of the fibrillar structure of the fibres can be controlled more easily than their microfibrillar structure.

Several important conclusions must be derived from the results and discussions of recent studies in fibre morphology. First, it is quite obvious that the structure of all fibres, and even of all melt-spun fibres, cannot be represented by the same model. The errors in such assumptions can be very large because it appears that the interaction between the microfibrils can vary considerably from fibre to fibre. Second, with melt-spun Nylon and PET fibres, where the interaction between the microfibrils is very large, it must be expected that the dimensions of crystallites and the characteristics of the macrolattice of these crystallites must have an important role in the mechanical and diffusive properties of fibres. Consequently, it is necessary to take these dimensions into consideration in theoretical treatments of modulus, diffusion, strength, etc. Finally, it must be recognized that not enough work has been performed on the analysis of the structure of the interfibrillar and intermicrofibrillar domains which have an important influence on fibre properties.

3. Diffusion

The control of the rate of dyeing and of the dye-uptake is one of the most challenging problems of textile technology; it is not surprising that the effects of fibre morphology on the diffusion characteristics of fibres attracted the attention of many authors during recent years.

The approach presented below had been influenced by the work of Bell [16] and Dumbleton *et al.* [17]. These authors showed the existence of very interesting correlations between (a) the diffusion coefficient and the imaginary modulus or viscosity of the sample, and (b) the diffusion and the morphological characteristics of the fibre. However, no attempts were made by these authors to treat the experimentally determined diffusion–imaginary modulus relationships explicitly in terms of fibre morphology. Since such analysis would help in clarifying the role of morphology on

diffusion, we refined their basic relationships to account for these effects. Our approach is based on the following considerations:

Fujita *et al.* [18] have shown that the diffusion coefficient D, in amorphous polymers in the rubber state is given by

$$\ln (D/RT) = -B \ln \eta + C \quad (1)$$

where R is the gas constant, T the absolute temperature, η is steady-state viscosity, and B and C are constants depending on the chemical structure of the polymer and penetrant. B is further expressed as

$$B = \frac{\Delta H_v}{\Delta H_B}. \quad (2)$$

ΔH_v and ΔH_B in Equation 2 are, respectively, the activation energies of viscous flow and diffusion. In cases where the size of the diffusing molecule is comparable to the size of the polymer segment that moves, $\Delta H_v = \Delta H_B$ and $B = 1$.

In the case of a semicrystalline polymer above the glass transition temperature, where the crystalline phase is essentially impermeable to diffusing molecules, the diffusion within the amorphous domain can still be expressed by Equation 1 in the form

$$\ln (D_a/RT) = -B_a \ln \eta_a + C_a \quad (3)$$

where the subscript a denotes that the particular quantities refer to amorphous phase only.

In the more complicated two phase system of semi-crystalline polymers, the diffusion processes may be described by the empirical equation

$$D = \phi_a^m D_a, \quad (4)$$

where ϕ_a is the degree of amorphicity, and m is a factor depending on the tortuosity of the permeable channels. Calculations, based on the geometrical features of the permeable and impermeable phase, show that m falls in the range between 0.3 and 1. Rewriting Equation 4 as

$$\ln (D/RT) = m \ln \phi_a + \ln (D_a/RT), \quad (5)$$

and combining Equation 5 with 3 we obtain

$$\ln (D/RT) = -B_a \ln \eta_a + C_a + m \ln \phi_a. \quad (6)$$

The amorphous viscosity η_a can be related to the measurable sample viscosity η, by

$$\eta = \phi_a^n \eta_a \quad (7)$$

where n is a constant related to the load transfer between the phases. From Equations 6 and 7 we have

$$\ln (D/RT) = -B_a(-n \ln \phi_a + \ln \eta) + C_a + m \ln \phi_a, \quad (8)$$

which can be rewritten as

$$\ln (D/RT) = -B_a \ln \eta + C_a + \ln (\phi_a^{m+nB_a}) \quad (9)$$

leading to the interpretation of diffusion results in terms of polymer structure. In Equation 9; (i) sample viscosity can be estimated from dynamic experiment by means of E''/ω, where ω = frequency in the experiment, (ii) C_a, B_a, ϕ_a, m and n are constants independent of temperature, (iii) with samples of the same amorphous orientation, B_a is independent of ϕ_a.

Prevorsek and Butler [19] applied Equation 9 to a series of experimental Nylon 6 fibres. The values of the various parameters in Equation 9 were obtained by analysing samples of (1) nearly equal viscosity and different amorphous content, (2) nearly equal viscosity and different amorphous content, but equal total and amorphous orientation, and (3) nearly equal amorphous content. Assuming the path of penetrating molecules to be approximately 1.5 times as long as it would be without the crystallites, the values of the parameters obtained were as follows:

$$m = 0.5$$
$$n = 0.68$$
$$B_a = 2.4$$
$$C_a = 30.3$$

Substituting these values into Equation 9 gives

$$\ln (D/RT) = -2.4 \ln (E''/\omega) + C_a + \ln \phi_a^{-1.12}. \quad (10)$$

In order to establish the accuracy of Equation 10 for describing the effects of fibre morphology on dyeing characteristics of Nylon 6 fibres, we selected 10 samples of various deformation and thermal histories, and carried out the necessary morphological and dyeing experiments. These results are summarized in Table III and Fig. 4. The plot of calculated and experimentally observed coefficients of diffusion shows an excellent correlation, supporting the validity of the concepts employed in the derivations of these expressions. It must be, however, recognized that there also are significant deviations from the predicted trend which this theory was unable to explain. In the

TABLE III Experimental Nylon 6 fibres; c_1 = dye uptake in 10 min, c_∞ = dye uptake at equilibrium, D = diffusion constant, proportional to $(c_1/c_\infty)^2$, E'' = loss modulus measured at 35° C, 95% r.h., 110 Hz, $\omega = 2\pi(1\,1\,0)$, ϕ_a = amorphous volume fraction.

Sample	$(c_1/c_\infty)^2 \sim D$	$\eta = E''/\omega$ (10^6 P*)	ϕ_a	f_a	f_c	Crystallite size (Å)	
						α_1	α_2
I	0.144	0.90	0.32	0.50	0.90	75	36
II	0.140	0.99	0.58	0.41	0.93	70	37
III	0.085	0.94	0.51	0.50	0.92	70	37
IV	0.073	1.07	0.46	0.50	0.89	70	36
V	0.107	0.92	0.43	0.50	0.89	66	36
VI	0.151	0.80	0.50	0.44	0.86	74	37
VII	0.262	0.63	0.53	0.44	0.86	72	36
VIII	0.460	0.72	0.52	0.34	0.89	70	36
IX	0.301	0.72	0.51	0.38	0.92	72	36
X	0.191	0.81	0.53	0.43	0.90	74	37

*$1P = 10^{-1}$ N sec m^{-2}.

search for a more accurate approach we decided to abandon the easy route via E'' because of its sensitivity to the dimensions of the crystallites and the characteristics of the macrolattice discussed in the section on modulus.

The expression for the coefficient of diffusion in terms of the crystallite dimensions and the spacing between the crystallites can be derived employing the method of Barrer and Petropoulos [20, 21]. This involves the treatment of diffusion in a lattice of identical rectangular parrallelpipeds embedded in a continuum described in Appendix 1.

This treatment leads to the following two expressions for the diffusion coefficients parallel, $D_\parallel$, and perpendicular, $D_\perp$, to the fibre axis

$$D_\parallel = \frac{hb(2a+b)D_A}{(a+b)^2 h_A(1+h_B/\beta h_A)} \qquad (11)$$

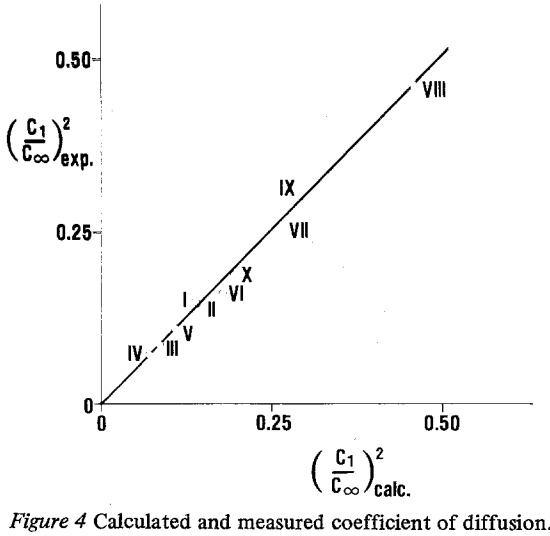

Figure 4 Calculated and measured coefficient of diffusion.

and

$$D_\perp = \frac{h_a b + h_b a + h_b b}{(a+b)a(1+b/\beta a)} D_A \qquad (12)$$

where

D_A = diffusion coefficient of the amorphous phase,
a = crystallite diameter,
b = lateral spacing between the crystallites,
h_a = crystallite height,
h_b = longitudinal spacing between the crystallites,
$h_a + h_b = h$ = long period,
β = coefficient related to nonparallel flow lines. We assume $\beta = 1$.

Thus, this approach requires the determination of the lateral spacing between the crystallites b, a quantity which has not yet been determined in fibres, and which reflects the volume fraction of the interfibrillar matter.

In the absence of an independent method to determine b, it is impossible at this stage to analyse the diffusion and dyeing responses of fibres in terms of morphological characteristics. This situation is particularly critical for the analysis of dyeing nonuniformities observed on thermal and mechanical treatments (such as texturing). There the chemical composition of the fibre remains essentially unchanged and variations in dyeing characteristics are primarily caused by changes in fibre morphology. It must be, therefore, recognized that the interpretation of dyeing results in terms of the variables of fibre structure is at this stage still inaccurate and the reported correlations may include a considerable error.

The use of Equations 11 and 12 above, on the other hand, permits the determination of b for systems where $D_\perp$ and $D_\parallel$ are experimentally determined. The application of this method to nylon fibres yields a spacing of 10 Å for fibres drawn 3 x, and 29 Å for fibres drawn 5.3 x.

These results have important implications on the mechanism of deformation between intermediate and high drawn ratios. In a drawing process where (1) the stretching of the microfibrils equals the macroscopic stretching of the fibre, and (2) the fibre is incompressible, the microfibril diameter and fibre length changes are related as follows;

$$D^2_{m,1}L_1 = D^2_{m,2}L_2 \qquad (13)$$

where D_m is the fibre diameter, L is the fibre length, and subscripts 1 and 2 denote the dimensions before and after drawing, respectively.

If one assumes that the SAXS width of the crystallites corresponds approximately to the width of the microfibril, then the crystallite width ratio of fibres drawn 3 x and 5.35 x should be in the order of $\sqrt{(5.35/3)} = 1.33$. The fact that the measured crystallite width ratio of 1.61 is much higher indicates that the microfibrils do not undergo the same degree of stretching as the fibre during this stage of drawing. A 3 x drawn fibre with microfibril diameter of 119 Å should lead to a microfibril diameter of 90 Å in a 5.35 x drawn fibre. This is 16 Å more than the experimentally observed value of 74 Å.

Thus, during drawing of nylon 6 fibre from 3 x to 5.35 x, the microfibrils do not stretch but slip past one another. This is based on the following findings: (1) The longitudinal structure of microfibrils (amorphous and crystallite length) remains essentially unchanged. (2) The microfibril thinning exceeds that of the fibre. (3) The spacing between the microfibrils increases. The microfibrils are sheared with respect to each other. The interfibrillar phase formed by the matter removed from the microfibrillar surfaces has a density similar to the average density of the microfibril. A model of this type of drawing is shown in Fig. 5.

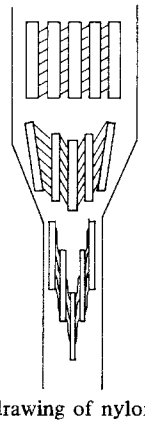

Figure 5 Model of drawing of nylon fibres between intermediate and high draw ratios.

4. Modulus

Bending and tensile moduli are very important textile properties [22–24]. Although the bending modulus appears in many equations describing the behaviour of fabrics and other textile structures, it is seldom determined in textile laboratories. Two principal problems are encountered in the determinations of bending modulus; (a) it is difficult to measure on long filament sections and (b) its determination is severely limited with fibres having non-uniform and non-circular cross-sections.

Several authors have investigated the relationships between bending and tensile moduli of fibres; it appears that these two properties are closely related and that for a given fibre it can be assumed that the bending modulus is proportional to tensile modulus. The proportionality constant between two properties, however, varies from fibre to fibre [22–24].

Since there is much more data available for the tensile than the bending modulus we shall limit the discussion of the effects of morphological and molecular variables on the tensile modulus.

The calculations of the modulus of elasticity corresponding to the principal chain direction of a polymer crystal of specified structure may be made from the force constants for bond-stretching and valence-angle deformation derived from vibration frequencies of molecules. Directional cosines and appropriate bond angles, and the packing of the chains in the crystals are derived from the X-ray data. The results obtained by Meyer and Lotmar [25], Lyons [26], Treloar [27] and Jaswon and coworkers [28], while based on calculations that neglect the effects due to interactions between polymer chains, are in most cases, in gratifying agreement with the crystal lattice moduli determined experimentally by Dulmage *et al.* [12] and Sakurada *et al.* [13] (In a recent article on the effect of hydrogen bonds on the axial stiffness of crystalline native cellulose, Gillis [29] introduced the significant influence of interchain primary bonds on deformational behaviour.)

The contribution of the moduli of the crystallites to the moduli of the semi-crystalline fibres is

affected by the type of load-transfer between the phases, which in turn depends on a variety of characteristics of the fibre structure. Many authors assume that, with respect to mechanical properties, the oriented polymers could be considered as a parallel array of microfibrils which are held together by a relatively weak interfibrillar matter. With this model, then, the modulus of the fibre is determined solely by the modulus of the microfibril, which in turn is determined by the combination of the moduli of the alternating amorphous and crystalline regions when they are loaded under conditions of equal stress (i.e. series load transfer). An important feature of this microfibrillar model, and the load transfer conditions which it implies, is that the fibre modulus is independent of the crystallite length to diameter ratio (i.e. aspect ratio).

An alternative mechanical model of a fibre involves the crystallites embedded in the "amorphous" matrix. In this case, the crystallite aspect ratio has a fundamental influence on the load transfer characteristics and thus the modulus of the fibre. For this model, equal stress (i.e. series) load transfer between the amorphous and crystalline regions is approached when the crystallites are platelets oriented perpendicular to the fibre axis. Other crystallite shapes (aspect ratios) give rise to different load transfer conditions.

A convenient means of determining which fibre model is more appropriate with respect to load transfer is to analyse the fibre modulus in terms of the moduli of the crystalline and amorphous regions. We have performed such an analysis on a series of Nylon 6 fibres of various draw ratios. Our analysis is based on the work of Takayanagi, who has shown that the mechanical response of two-phase systems may be represented by means of unit cube models [30].

In this representation the fibre modulus E_f is given by

$$E_f = \lambda[\phi/E_c + (1-\phi)/E_a]^{-1} + (1-\lambda)E_a \quad (14)$$

where E_c and E_a are the respective moduli of crystalline and amorphous domains of the fibres, and $\lambda\phi = X$ = degree of crystallinity.

The model has two extreme responses. When $\lambda = 1$ the response is in series (or equal stress); when $\phi = 1$ the response is in parallel (or equal strain). With isotropic semi-crystalline polymers $\lambda \approx \phi < 1$, while an isolated microfibril is expected to yield a series response (i.e. $\lambda = 1$).

In order to apply this method in determining the appropriate model (i.e., the values of λ and ϕ) it is necessary to determine E_f, E_c, E_a and the degree of crystallinity, X.

In our study, the fibre modulus was measured directly on a dynamic-viscoelastometer at 110 Hz. The fibres were characterized by wide-angle X-ray diffraction to determine the degree of crystallinity and the crystalline orientation function. The amorphous orientation function was estimated from X-ray and birefringence data using the method of Stein [31]. Estimates of the effective crystalline modulus were made from the works of Dulmage *et al.* [12] and Sakurada *et al.* [13] noted previously together with the experimentally determined crystalline orientations. In order to estimate the effective amorphous modulus for each fibre in the series, we assumed that the modulus of the amorphous phase of the fibre of orientation f_a was equal to that of an "amorphous" fibre (as determined by wide-angle X-ray) of the same orientation.

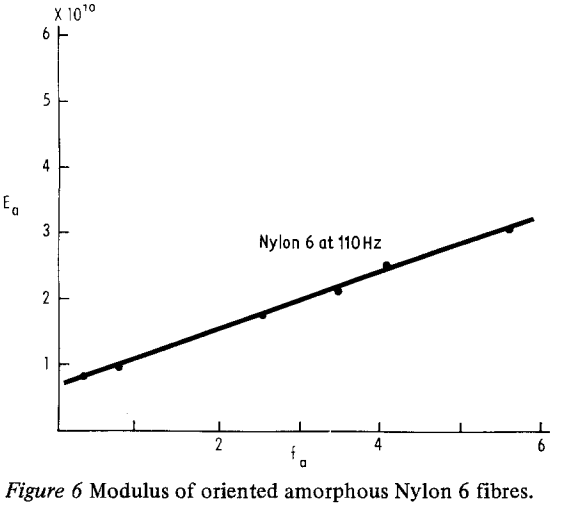

Figure 6 Modulus of oriented amorphous Nylon 6 fibres.

TABLE IV Vertical (ϕ) and horizontal (λ) dimensions of the mechanical analog

	E_f (dyne cm^{-2}) × 10^{10}	X (%)	E_c (dyne cm^{-2}) × 10^{10}	λ	ϕ	E_a (dyne cm^{-2}) × 10^{10}	$\frac{\phi}{\lambda}$
1 ×	2.35	0.63	12	0.80	0.787	0.70	0.98
3 ×	4.80	0.56	25	0.98	0.570	2.34	0.58
5.35 ×	5.50	0.34	25	0.52	0.654	3.26	1.26

In the absence of data relating the amorphous modulus of Nylon 6 to orientation we prepared a series of "amorphous" fibres of different orientations (as determined from birefringence data using $\Delta_a^0 = 0.073$) and measured their moduli at 110 Hz. The data for these specially prepared "amorphous" fibres is plotted in Fig. 6.

With the necessary estimates of the required quantities in hand, we proceeded to determine the vertical (ϕ) and the horizontal (λ) dimensions of the general mechanical model represented by Equation 14. These results are given in Table IV.

These calculations showed that only the fibres of intermediate draw ratio exhibit a series response ($\lambda \approx 1$, equal stress between phases) which is consistent with the microfibrillar fibre model. For fibres of draw ratio of 5.3 ×, λ is considerably less than 1. Thus, it was concluded that the microfibrillar model does not adequately represent this system [6].

In order to estimate the effective length to diameter ratio of the crystallites in the 3 × and 5.3 × fibres we employed equations derived by Halpin and Tsai [32] shown below. These equations may be applied to two phase systems in which the higher modulus reinforcing elements (i.e. the crystallites) are embedded in a matrix (i.e. the amorphous material) and are perfectly aligned with respect to the applied load.

$$E_f = [1 + U\eta X)/(1 - \eta X)]E_a \qquad (15)$$

where

$$\eta = (E_c/E_a - 1)/(E_c/E_a + U)$$

$$U = 2(l/d)^*,$$

$$l, d = \text{length, diameter of crystallites,}$$

and X = degree of crystallinity.

The calculations of the fibre modulus as a function of the crystallite aspect ratio for the 3.0 × and 5.35 × fibres lead to the following results. The crystallite aspect ratio for the 5.35 × fibre corresponding to its (measured) modulus is about $\frac{1}{2}$, while the length to diameter ratio for the 3.0 × fibre is less than $\frac{1}{50}$. In other words, the crystallites in the low draw ratio fibre are shaped like platelets oriented perpendicular to the fibre axis, while for the higher draw ratio, the crystallites approach the shape of cubic particles. These estimates of the crystallite shapes do not agree with crystallite dimensions obtained from wide-angle X-ray analysis and small-angle X-ray long-period estimates, since these analyses imply that, in drawing fibres from 3.0 to 5.35 ×, only a small decrease in crystallite width occurs.

In order to resolve this discrepancy between the mechanical and crystallographic analyses, we obtained additional information on the crystallite dimensions by employing the small-angle X-ray methods of Harget [33], and Gezalov [34]. These studies indicated that drawing from 3.0 × to 5.35 × has little influence on the crystallite size in the direction of orientation, and that the crystallite width decreases significantly from 119 Å for the 3 × fibres to 70 Å for the fibres drawn 5.35 ×. The crystallite aspect ratios for the fibres estimated from the SAXS and the modulus analyses are shown in Table V. The results indicate a qualitative agreement, in that both methods indicate an increase in aspect ratio with increased draw ratio. Quantitative agreement is fair for the 5.3 × fibres, but for the low draw ratio fibres, the discrepancy is too large to be ignored.

TABLE V Crystallite aspect ratios from SAXS and modulus data

Draw ratio	SAXS	Modulus analysis
3 ×	0.48	0.02
5.3 ×	0.8	0.5

The difference in l/d could result from the fact that (1) neither of the two models adequately represents the state of stress in these fibres, or (2) the crystallites in the fibres of low draw ratio are so close that the crystals are mechanically coupled across their boundaries. In order to explore this second hypothesis it was necessary to determine the spacing between the crystallites. This parameter was obtained by means of diffusion analysis described above.

According to this analysis the lateral spacing between the crystallites in Nylon 6 fibres drawn 5.3 × is almost three times as that in the same fibres drawn 3 ×. On the basis of these results, and SAXS data which indicate that the crystallites in these fibres are arranged in planes perpendicular to the fibre axis, it was postulated that in fibres drawn 3 × the relative displacement is inhibited by

*In comparing Equations 14 and 15 it is important to note that the parameters ϕ and λ of Equation 14 are not closely related to the dimensions of crystallites l and d appearing in Equation 15. This can be best illustrated by comparing $2\phi/\lambda$ and U for some values of E_a, E_c and X as shown in Appendix 2.

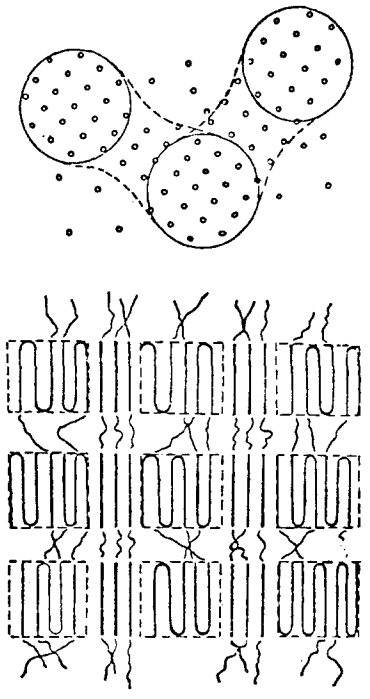

Figure 7 Model of microfibril fusion via epitaxial crystallization of extended chain molecules.

a narrow junction where two crystallites are fused. A recent electron microscopy study with Nylon 6 fibres stained with $SnCl_2$ support the view that the crystallites in adjacent microfibrils may be fused as shown schematically in Fig. 7.

These results clearly show that the modulus is not a function of amorphous and crystalline orientation as assumed by several investigators. The neglect of the role of crystallite dimensions and the characteristics of the crystalline macrolattice can lead to significant errors in the interpretation of the results or in the prediction of properties on the basis of morphological characteristics of the fibre.

The effect of heat-setting on modulus is probably as important as that of draw ratios when the analysis of textile performance is the consideration. Heat-setting is frequently a necessary and important step in the manufacturing of fabrics. It is well known that heat-setting leads to a marked difference in the wrinkling behaviour of fabrics and part of this effect is associated with the change in the fibre modulus.

In the analysis of the effects of heat-setting on fibre structure and modulus, it is necessary to take into consideration the role of pretension or degree of shrinkage (or extension) during the heating of fibres (or fabrics). On the results of Stratton *et al.* [35] and McGraw [36], and the data presented below, it is quite clear that pretension has an important effect on the magnitude and the rate of structural and property changes during heat-treatments. In general, the changes in modulus and structure are much less when the heat-treatments are carried out under high pretension (or low shrinkage), than under conditions where the samples are free to contract.

The effect of shrinkage on fibre morphology and modulus was recently investigated by Prevorsek *et al.* [11] in a series of experiments, where a series of PET fibres of various molecular weights were first drawn to a practical maximum draw ratio, and then allowed to contract thermally under tension for 10, 20 and 38%. The contraction was carried out by passing the fibres over a heating block kept at 225° C. The respective contact times of fibres with the heating block were 3.16, 3.33 and 3.70 sec for experiments leading to 10, 20 and 38% contraction. The tensions on the yarn during the contraction step, however, varied from 150 to 15 g for the experiments involving 10 and 38% contraction.

The molecular weights and drawing extension of fibres subjected to these experiments are summarized in Table VI while the moduli at 23 and −100° C are presented in Table VII.

These results show that, in general, contraction leads to a decrease in modulus and amorphous orientation as observed by previous workers [5]. However, the correlations between degree of contraction and modulus, and amorphous orientation and modulus may not be as simple as indicated. Although the modulus decreases monotonically with increasing contraction both at 23 and −100° C the two sets of data reveal marked differences in the dependence of modulus on the degree of contraction. Note, for example, that contraction from 0 to 10% leads to an average decrease in modulus from 300 to 190 (~34%) at −100° C, whereas the decrease at 23° C is from 202 to 165 (~19%). The trend is, however, reversed in the contraction range from 10 to 20%, where the change is larger at 23° C (~30%) than at −100° C (~9%).

Similar differences exist in the variation of modulus with amorphous orientation. Thus, for example, a contraction from 20 to 38% has no effect on the amorphous orientation function but the modulus decreases by about 45% at 23° C and 60% at −100° C.

TABLE VI Number-average molecular weights and drawing extensions of experimental PET fibres

Sample	$\bar{M}_n$ (× 10^4)	Drawing extension, $\Delta L/L \times 100$
I	1.33	480
II	2.11	500
III	2.63	560
IV	3.05	530

This last observation is particularly important because several studies reported in the literature indicate surprisingly good correlations between properties and values of amorphous orientation functions [5]. We investigated these relationships on several occasions, and found that frequently f_a gives a good correlation with properties. However, there are also numerous exceptions to this and, therefore, we discourage the use of this function to correlate fibre properties with morphology.

The failure of orientation functions to explain modulus is not surprising in view of numerous changes in the fibre structure which take place during thermal contraction. The summary of these changes is given in Table VIII.

On the basis of the above results it can be concluded that heat setting leads to a decrease in modulus and that the magnitude of the effect increases with increasing temperature, time of heat-setting as well as the degree of contraction of fibres during this operation.

5. Strength

In order to establish the morphological factors which affect fibre strength, we must examine the structural models of PET and Nylon 6 fibres shown in Figs. 2 and 3. In addition we take into consideration the structural changes occurring during drawing, discussed above. Since in this process the microfibrils are not stretched but rather slip past one another, it is assumed that in this phase of drawing the strength of the microfibrils remains essentially unchanged. The relative displacement of microfibrils involves the removal of the matter from the surfaces of the microfibril which leads to the formation of a highly extended interfibrillar phase. The density of these extended-chain phase is similar to the average density of the microfibril. Thus, it can be assumed that the order of these domains is higher than that of the amorphous domains in the microfibril and less than that of the crystallites of the microfibril. Because the interfibrillar domain consists predominantly of extended-chain molecules, it represents the strongest phase of the fibre structure. On the basis of IR data indicating a considerable amount of regular chain-folding, we believe that the microfibrils are relatively weak probably in the order of $\sim 2\,g\,den^{-1}$ * for Nylon 6.

The amorphous domains of the microfibril are the weakest element of fibre structure and are re-

*9 den = $1\,g\,km^{-1}$

TABLE VII Experimental PET fibres

Degree of contraction (%)	Sample	f_a	Modulus ($g\,den^{-1}$) and average variation					
			+ 23° C			−100° C		
			Modulus	Average*	Change (%)†	Modulus	Average*	Change (%)†
0	I		198			293		
	II		205			298		
	III		202	202		301	300	
	IV	0.729	205		19	306		34
10	I		155			178		
	II		162	165		182	191	
	III		167			196		
	IV	0.565	178		30	208		9
20	I		108			168		
	II		109	114		170	175	
	III		118			175		
	IV	0.448	120		46	187		60
38	IV	0.448	64.8			73.5		

*Average of the four values in the preceding column.
†Percentage change in the average values between two successive levels of contractions.

TABLE VIII Summary of changes in structure during various phases of thermal contraction

Degree of contraction	Structural changes
0–10%	A decrease in the L.P. from 190 to 163 Å A decrease in amorphous orientation function from 0.729 to 0.565 An increase in the regular chain folding* An improvement in the lateral order in the crystallites† An increase in the electron density difference between the crystalline and amorphous domains‡ An increase in the lateral order of the macrolattice §
10–20%	A decrease in amorphous orientation from 0.565 to 0.448 A marked increase in the degree of regular folding* A small increase in degree of crystallinity An improvement in macrolattice lateral order § A small increase in electron density difference‡ No change in L.P. and lateral order of crystallites
20–38%	A small but significant decrease in the degree of crystallinity A decrease in the degree of regular chain-folding* A decrease in the intensity of the small-angle pattern No significant changes in the long period and the four-point angle No change in the amorphous orientation function and a relatively small decrease in the crystalline orientation function

*As indicated by the intensity changes of the 988 cm^{-1} band.
†As indicated by the increase in the effective width of the crystallites.
‡As indicated by the intensity changes of the small-angle X-ray scattering.
§As indicated by the changes in the width of the spots in the small-angle X-ray pattern.

garded as the precursors of the macroscopic crack which leads to fibre rupture. The existence of this elementary crack, whose dimensions are similar to the microfibril diameter, were recently demonstrated by transmission electron microscopy using thin stained cross-sections of Nylon 6 [10]. From photomicrograph of a highly drawn Nylon 6 fibre stained with $SnCl_2$, we estimated that the diameter of the dark spots indicating the microcracks is about ~ 75 Å which agrees well with the value of the microfibril diameter derived from SAXS analysis by Harget (74 Å) [6]. In addition, this photomicrograph provides also the number of microcracks per unit area which is related to the concentrations of the crack nucleation sites, Z, which appears in the Prevorsek–Lyon theory of strength. The number of the amorphous domains per unit cross-sectional area determined by this technique is $\sim 2.4 \times 10^{11}$ cm^{-1} [10].

From this result and the dimensions of the long period of 90 Å, we obtain the concentration of the crack nucleation site to be in the order of 2.6×10^{17} cm^{-3} which is sufficiently close to the concentration of free radicals formed in the breakage of Nylon 6 fibres. This result shows that, in the process of fibre breakage, these microcracks do not grow, but that a minimal amount of chain scission is required to reach the conditions under which these cracks become unstable and propagate catastrophically across the specimen. These findings support the validity of the crack stability criteria applied by Prevorsek [37–39]. In the theory of fibre strength, this author uses the stability criteria for an elastic circular crack, derived by Sack [40],

$$r^* = \frac{\pi\rho E}{2(1-\mu^2)q^2\sigma^2} \qquad (16)$$

There, r^* = radius at which the crack becomes unstable, E = modulus, ρ = fracture surface energy, μ = Poisson's ratio, q = stress concentration factor and σ = stress. Using the following values of these parameters for Nylon 6 which were either calculated (calc) or measured (exp), $E_{exp} = 0.7 \times 10^{11}$ dyne cm^{-2}, $\mu_{exp} = 0.4$, $\sigma_{exp} = 0.35 \times 10^{10}$, $\rho = 1600$ erg cm^{-2} and $q_{calc} = 4.2$ one finds that the critical size of the crack is in the order of 77 Å.

Since the critical crack size for this case (r^* = 77 Å) is of the same magnitude as the size of the pre-existing flaws in the microfibril (74 Å) it follows that these cracks cannot grow significantly during straining to rupture.

These conclusions are supported by recent studies of Reimschuessel and Prevorsek with strained Nylon 6 fibres using transmission electron microscopy. These investigations showed that the microcracks of fibres subjected for short periods of time to stresses amounting to 0.95% of their strength are of the same dimensions as the microcracks in the samples before straining.

The structural model used in the analysis of fibre strength is shown in Fig. 8. The calculation proceeds in two steps; (1) The calculations of the concentration factor associated with fibre morphology, i.e. with the ensemble of cracks shown

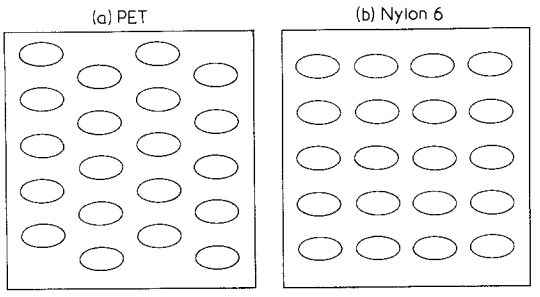

Figure 8 Model of fibre strength; (a) PET, (b) Nylon 6.

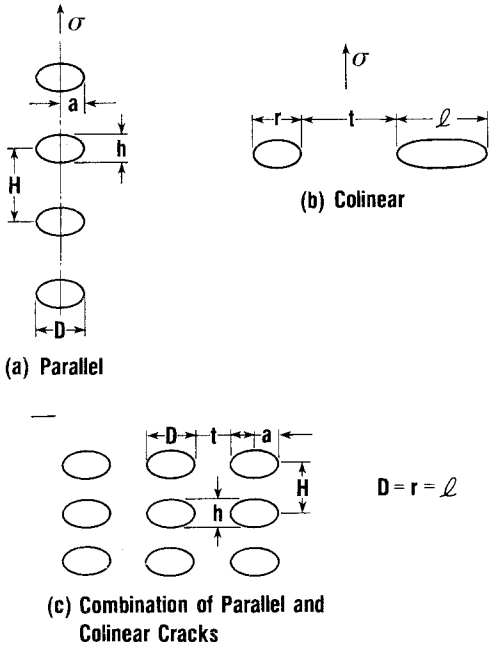

Figure 9 Ensemble of cracks.

in Fig. 9, and (2) the calculations of the strength of a parallel ensemble of extended polymer chains which constitute the interphase between the microfibrils. Pertinent morphological data for a high and a low draw ratio Nylon 6 fibre are given in Table IX. The stress concentration factor associated with an elliptical hole corresponding to the amorphous domain of the low draw ratio fibre is obtained using

$$Q = 1 + 2D/h \qquad (17)$$

where Q = stress concentration factor, D = diameter of the crack and h is the height of the crack. With the low draw ratio fibre $Q = 9.0$ (See Fig. 9a).

Interactions between equally spaced parallel cracks were studied by Koiter [41] and Yokobori

TABLE IX Nylon 6 model and dimensions (Å) (c.f. Fig. 9)

	Low draw ratio	High draw ratio
$D (= l = r)$	119	74
t	10	29
H	89	93
h	30	32

[42]. Theoretical calculations predict that a specimen with an infinite number of equivalent and equal size parallel cracks is stronger than that containing only one crack of same size. The expression describing this case has the following form.

$$\frac{\sigma_\infty}{\sigma_1} = \left[1 - \frac{1}{2}\left(\frac{\pi a}{H}\right)^2 + \frac{3}{8}\left(\frac{\pi a}{H}\right)^4 + \ldots\right]^{-1}. \qquad (18)$$

In the absence of closed form solution for values of a/H observed with fibres of this study, it was necessary to determine σ_∞/σ_1 by the following experimental technique.

On one test specimen, only one crack was made and on another specimen many cracks were made and the tensile strength of the two specimens were compared. This study showed that in the entire range of a/H investigated, the samples having an array of cracks are substantially stronger than those having only one crack. From these studies, we obtained σ_∞/σ_1 corresponding to low and high draw ratio nylon fibres to be 1.53 and 1.55, respectively. Values of parameters used in these calculations are given in Table IX.

Next we calculated the concentration of stress for a specimen containing an infinite number of collinear cracks. The calculations and experimental data show that the presence of additional cracks in collinear arrangement weakens the specimen. However, the degree of weakening is not very sensitive to the number of cracks. Thus the ratio of strength of a sample having one isolated crack to that having an infinite number of such cracks in collinear arrangement can be approximated by σ_2/σ_1 where σ_2 is the strength of the sample having 2 such cracks.

The stress concentration factor for a system containing 2 cracks as shown in Fig. 9b is given by

$$\frac{\sigma_1}{\sigma_2} = \frac{l - (l+t)\,[K(k) - E(k)]\,/K(k)}{\sqrt{(l)}\sqrt{(lt/(r+t)}} \qquad (19)$$

where

$$k = \sqrt{\frac{lr}{(t+l)(t+r)}},$$

and $K(k)$ and $E(k)$ are the complete elliptic integrals of the first and second kind.

For the crack geometry and spacings of the low draw ratio fibre, $\sigma_1/\sigma_2 = 1.55$.

The total stress concentration factor for the cracks shown in Fig. 9c is then obtained by multiplying all three contributions:

$$q = Q\left(\frac{\sigma_1}{\sigma_2}\right)_{\text{colinear}}\left(\frac{\sigma_1}{\sigma_\infty}\right)_{\text{parallel}},$$

which leads to $q = 9.1$. A similar procedure applied to the characteristic of the high draw ratio fibre leads to a value of $q_{\text{total}} = 4.2$.

Thus, these calculations predict that the strength of the high draw ratio fibre would be about twice as high as that of the low draw ratio fibre, in excellent agreement with the experimental results.

The strength of uniaxially oriented polymers is, therefore, estimated from the strength of the extended chain domains, and the stress intensity factor associated with the presence of the microcracks in the system. The parameters affecting the stress intensity factors are the crack length, the distance between the cracks, and the radius of curvature at the tip of the microcrack.

The values of these parameters are closely related to the dimensions of the crystallites (width and length, the length of the amorphous domain, and the distance between the microfibrils).

On the basis of this analysis it can then be concluded that the increase in strength on drawing results from:

(1) the increase of the volume fraction of the interfibrillar extended-chain domain, and

(2) the decrease in stress concentration factor at the tip of the microcrack which is associated with the decrease in the crystallite width and the increase in the distance between the crystallites.

Appendix 1
Derivation of diffusion equations

This derivation involves the treatment of diffusion in a lattice of identical rectangular parallelpipeds embedded in a continuum. The parallelpipeds may be parallel with or normal to the direction of flow. Figs. 10a and b show the arrangement in side and end-on section of the parallelpipeds and Fig. 10c shows parts of a chain of parallelpipeds in the continuum. The problem involves the evaluation of the flux down a single chain. The flow through the chain is considered as that through a smaller chain of cross-section a^2, and composed of alternating crystalline and amorphous regions A and B of length h_A and h_B, respectively, and a surrounding hollow tube of square cross-section of area $(a+b)^2 - a^2 = b(2a+b)$. Flows through the cross-section a^2 at the mid-point of A and B are, respectively, J_A and J_B and the corresponding flows in the surrounding hollow shell are J'_A and J'_B.

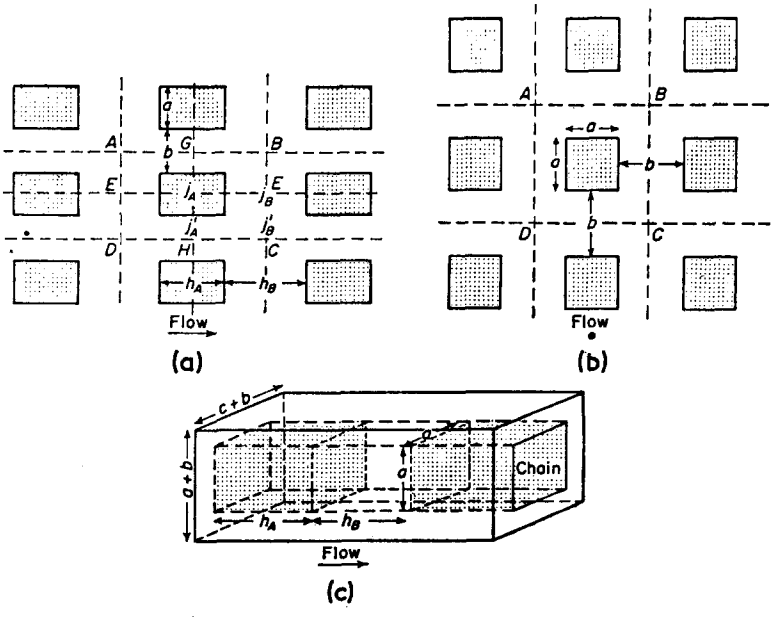

Figure 10 Geometrical details of the lattice of rectangular parallelpipeds. Part A = side view, Part B = end-on-view. Phase A = ▦, Phase B = □.

Because of non-parallelism of flow lines with the chain, J_A and J_B are non-equal, but instead

$$J_A = \gamma J_B, \tag{A1}$$

where γ is a coefficient.

J_A and J_B are related to the mean fluxes $\bar{J}_A$ and $\bar{J}_B$ by

$$J_A = \beta_A \bar{J}_A$$

and

$$J_B = \beta_B \bar{J}_B$$

where β_A and β_B are coefficients because of the non-parallel flow lines. If $(C_{A1} - C_{A2})$ and $(C_{B1} - C_{B2})$ represent the concentration differences between the upstream and downstream faces of A and B, then

$$J_A = \beta_A \bar{J}_A = \beta_A a^2 D_A (C_{A1} - C_{A2})/h_A \tag{A2}$$

and

$$J_B = \beta_B \bar{J}_B = \beta_B a^2 D_B (C_{B1} - C_{B2})/h_B, \tag{A3}$$

where D_A and D_B are, respectively, the diffusion coefficients of phase A and phase B.

If l is the length of the chain and n is the number of cells of phase A and phase B in the chain, then

$$l = n(h_A + h_B) = nh. \tag{A4}$$

The total concentration drop across the composite membrane as measured in phase A is then

$$\Delta C_A = n(C_{A1} - C_{A2}) + nK(C_{B1} - C_{B2}) \tag{A5}$$

where equilibrium exists at each interface, described by Henry's Law Constant K. Then from Equations A1, A2, A3, and A5

$$\Delta C_A = n(C_{A1} - C_{A2}) \left(1 + \frac{\beta_A h_B K D_A}{\beta_B h_A \gamma D_B}\right). \tag{A6}$$

The surrounding tube of B is also divided into cells of length h_A and h_B, alternatively, corresponding with the cells A and B in the central chain. Defining mean fluxes $\bar{J}'_A$ and $\bar{J}'_B$ in terms of the concentration differences $(C'_{A1} - C'_{A2})$ and $(C'_{B1} - C'_{B2})$ along the lengths of h_A and h_B of surrounding tube, we have

$$\begin{aligned} J'_A = \beta'_A \bar{J}'_A &= \beta'_A \frac{b(2a+b)D_B}{h_A} (C'_{A1} - C'_{A2}) \\ &= \gamma' J'_B = \gamma' \beta'_B \bar{J}'_B \\ &= \frac{\gamma' \beta'_B b(2a+b) D_B}{h_B} (C'_{B1} - C'_{B2}) \end{aligned} \tag{A7}$$

where β'_A, γ', β'_B are coefficients. The total concentration drop across the composite membrane as measured in phase B is then

$$\Delta C_B = n(C'_{A1} - C'_{A2}) + n(C'_{B1} - C'_{B2}) \tag{A8}$$

From Equation A7

$$n(C'_{B1} - C'_{B2}) = n(C'_{A1} - C'_{A2}) \left(\frac{B'_A h_B}{\gamma' h_A \beta'_B}\right) \tag{A9}$$

Substituting Equation A9 into Equation A8

$$\Delta C_B = n(C'_{A1} - C'_{A2}) \left(1 + \frac{B'_A h_B}{\gamma' h_A \beta'_B}\right). \tag{A10}$$

Because of steady-state conditions

$$\Delta C_A = K \Delta C_B, \tag{A11}$$

and

$$J_A + J'_A = J_B + J'_B,$$

from Equation A7 $\gamma J_B + \gamma' J'_B = J_B + J'_B$,

$$J_B / J'_B = \frac{1 - \gamma'}{\gamma - 1} \tag{A12}$$

The overall flux, J, through the cross-section ABCD in Figure 5b is then the sum of the fluxes through a cross-section of the central chain and the surrounding tube $(J = J_A + J'_A = J_B + J'_B)$ and is related to the overall concentration drop ΔC_B in the continuous phase by (cf Equations A2 and A3)

$$J = (a+b)^2 \bar{D} \frac{\Delta C_B}{l} \tag{A13}$$

where $\bar{D}$ is the mean overall diffusion coefficient. By combining Equations A2, A7, A11, A12 and A13, we obtain

$$\begin{aligned} \bar{D} &= \frac{Jl}{(a+b)^2 D C_B} = \frac{Jnh}{(a+b)^2 \Delta C_B} \\ &= \frac{h}{(a+b)^2} \left(\frac{nJ_A}{\Delta C_B} + \frac{nJ'_A}{\Delta C_B}\right) \end{aligned}$$

$$\begin{aligned} \bar{D} = \frac{h}{(a+b)^2} \Bigg[&\frac{n\beta_A a^2 D_A (C_{A1} - C_{A2})}{h_A \Delta C_B} \\ &+ \frac{n\beta'_A b(2a+b) D_B (C'_{A1} - C'_{A2})}{h_A \Delta C_B} \Bigg] \end{aligned}$$

$$= \frac{h}{(a+b)^2}\left[\frac{a^2\beta_A KD_A}{h_A + \dfrac{\beta_A h_B KD_A}{\beta_B \gamma D_B}} + \frac{b(2a+b)\beta'_A D_B}{h_A + \dfrac{\beta'_A h_B}{\beta'_B \gamma'}}\right] \quad \text{(A14)}$$

Thus, this is the general form of the equation describing the diffusion in a two-phase system.

In the case of a semi-crystalline polymeric fibre phase A, the crystallites are essentially impermeable to the diffusion of dye molecules, whereas phase B the amorphous component is permeable. In such a system, $KD_A \to 0$ and $\beta'_A \to 1$ so that the first term of Equation A14 becomes zero; h_A is the crystallite height, h_B is the longitudinal spacing between the crystallites; $h_A + h_B = h$ is long period; b is the lateral spacing between the crystallites; D_B can be replaced by D_A the diffusion coefficient of the amorphous phase. $D_\parallel$, the diffusion coefficient parallel to the fibre axis is then given by

$$D_\parallel = \frac{hb(2a+b)D_A}{(a+b)^2 h_A(1 + h_B/\beta h_A)} \quad \text{(A15)}$$

where $\beta = \beta'_B\gamma'$ is a coefficient related to non-parallel flow lines.

For a case of diffusion in a direction perpendicular to the fibre axis reference to Fig. 10a and b shows that the crystallite area of cross-section is $h_A a$ and the surrounding tube area of cross-section is $(h_A + b)(a+b) - h_A a$ or $h_A b + ba + b^2$.

Substitution of these values of dimensions in Equation A15 gives the diffusion coefficient in a direction perpendicular to the fibre axis, $D_\perp$ as

$$D_\perp = \frac{h_a b + h_b a + h_b b}{(a+b)a(1 + b/\beta a)} D_A \quad \text{(A16)}$$

Appendix 2
Relation between parameters ϕ and λ of Takayanagi's unit cube model and crystallite dimensions l and d

Takayanagi has shown that the mechanical responses of two-phase systems can be represented very accurately by means of a unit cube model.

According to this model, the system modulus E_f is given by

$$E_f = \lambda \Big/ \left(\frac{\phi}{E_c} + \frac{1-\phi}{E_a}\right) + (1-\lambda)E_a, \quad \text{(A17)}$$

where E_c and E_a are the respective moduli of the crystalline and amorphous phase and ϕ and λ are the dimensions of the crystalline domain in the model. The product $\phi\lambda$ equals the degree of crystallinity. The scope of this appendix is to establish whether there is a correlation between the crystalline domain of the model and actual dimensions of the crystallite i.e. crystallite aspect ratio l/d.

Using the Halpin–Tsai equation, which has been verified several times in composite structures, as a point of reference, we must establish the relationship between ϕ and λ in Equation A17 and parameter U in

$$E_f = \frac{E_a(1 + U\eta X)}{1 - \eta X}, \quad \text{(A18)}$$

where

$$\eta = \left(\frac{E_c}{E_a} - 1\right) \Big/ \left(\frac{E_c}{E_a} + U\right) \quad \text{(A19)}$$

$$U = 2\frac{l}{d} \quad \text{(A20)}$$

By combining Equations A17 and A18, and substituting for λ with X/ϕ, we obtain

$$\frac{X/\phi}{\dfrac{\phi}{E_c} + \dfrac{1-\phi}{E_a}} + \left(1 - \frac{X}{\phi}\right)E_a = \frac{E_a(1 + U\eta X)}{1 - \eta X}. \quad \text{(A21)}$$

Division of both sides with E_a and substitution for E_c/E_a with ζ leads to

$$\frac{X/\phi}{\dfrac{\phi}{\zeta} + 1 - \phi} + 1 - \frac{X}{\phi} = \frac{1 + U\eta X}{1 - \eta X}. \quad \text{(A22)}$$

Since

$$\eta = (\zeta - 1)/(\zeta + U),$$

Equation A22 can be rewritten as

$$\frac{1 + \left(\dfrac{\zeta - 1}{\zeta + U}\right)UX}{1 - \left(\dfrac{\zeta - 1}{\zeta + U}\right)X} = C \quad \text{(A23)}$$

where

$$C = \frac{X/\phi}{\dfrac{\phi}{\zeta} + 1 - \phi} + 1 - \frac{X}{\phi} = \frac{E_f}{E_a}. \quad \text{(A24)}$$

This substitution gives

$$U = \frac{(\zeta - \zeta X + X)C - \zeta}{1 + \zeta X - X - C} \quad \text{(A25)}$$

The Equation A25 correlates the crystallite aspect ratio l/d (in terms of U) with the Tabayanagi parameters ϕ and λ which are included in C.

As a numerical example we consider the case where $\zeta = E_c/E_a = 100$ and $X = 0.5$.

The choice of these values is suitable for semi-crystalline fibres such as PET, Nylon 6 and Nylon 66. Under these conditions,

$$C = \frac{0.5/\phi}{1 - 0.99\phi} + 1 - \frac{0.5}{\phi}$$

and

$$U = \frac{50.5C - 100}{50.5 - C}$$

TABLE A-I Values of E_f/E_a, $2l/d$, λ, and $2\phi/\lambda$ as function of ϕ: $E_c/E_a = 100$, degree of crystallinity X = 0.5

ϕ	$C (= E_f/E_a)$	$U (= 2l/d)$	λ	$2\phi/\lambda$
0.1	1.55	*	5.0	0.04
0.2	1.62	*	2.5	0.16
0.3	1.70	*	1.7	0.35
0.4	1.83	*	1.25	0.64
0.5	2.0	0.01	1.0	1.0
0.6	2.22	0.29	0.83	1.45
0.7	2.61	0.67	0.71	1.96
0.8	3.38	1.50	0.63	2.54
0.9	5.54	4.0	0.55	3.28
1.0	50.5	∞	0.50	4.0

*Equation A18 yields negative values for U, so these solutions do not have a physical meaning.

Values of $C(= E_f/E_a)$, $U(= 2l/d)$, λ, and $2\phi/\lambda$ corresponding to values of ϕ between 0.1 and 1 are tabulated in Table A-I. This calculation shows that under these conditions, Equation A18 yields the results which have a physical meaning only for values of $0.5 \leqslant \phi \leqslant 1$. When $\phi = 0.5$ the aspect ratio of crystallites is 0.01 while ϕ/λ is 0.5. With $\phi = 1$, l/d becomes infinity while $\phi/\lambda = 2$. The main difference between the values of ϕ/λ and l/d is therefore in their limits. The variations in l/d range from 0 to ∞, while ϕ/λ varies only from 0.5 to 2.

Acknowledgment

Dr Paul Harget and Mrs A. Reimschuessel provided data which were essential in the preparation of this article.

References

1. A. PETERLIN, *J. Polymer Sci. C* **13** (1971) 133.
2. K. SAKAOKU and A. PETERLIN, *ibid A-2* **9** (1971) 895.
3. A. PETERLIN and K. SAKAOKU, *J. Appl. Phys.* **38** (1967) 4152.
4. R. J. SAMUELS, *J. Macromol. Sci. -Phys.* **B4** (1970) 701.
5. *Idem, J. Polymer Sci. A-2* **10** (1972) 781.
6. D. C. PREVORSEK, P. J. HARGET, R. K. SHARMA and A. C. REIMSCHUESSEL, *J. Macromol. Sci. -Phys.* **B8 1–2,** (1973) 127.
7. P. BARHAM and A. KELLER, *J. Polymer Sci. Letters* **13** (1975) 197.
8. D. C. PREVORSEK and A. V. TOBOLSKY, *Textile Res. J.* **33** (1963) 795.
9. A. PETERLIN, *J. Macromol. Sci. -Phys.* **B6(4)** (1971) 583.
10. A. C. REIMSCHUESSEL and D. C. PREVORSEK, *J. Polymer Sci. A-2* **14** (1976) 485.
11. D. C. PREVORSEK, G. A. TIRPAK, P. J. HARGET and A. C. REIMSCHUESSEL, *J. Macromol. Sci. -Phys.* **B9(4)** (1974) 733.
12. W. J. DULMAGE and L. E. CONTOIS, *J. Polymer Sci.* **28** (1958) 275.
13. I. SAKURADA, I. ITO and K. NAKAMAΣ, *ibid C* **15** (1966) 75.
14. See for example, U.S. Patents 3 387 305, 3 457 609, and 3 499 822.

14a. See, for example, U.S. Patent 3 506 535.

15. N. V. HIEN, S. L. COOPER and J. A. KOUTSKY, *J. Appl. Polymer Sci.* **12** (1968) 2709.
16. J. P. BELL, *ibid* **12** (1968) 627.
17. J. H. DUMBLETON, J. P. BELL and T. MURAYAMA, *ibid* **12** (1968) 2491.
18. H. FUJITA, A. KISHIMOTO and K. MATSUMOTO, *Trans. Faraday Soc.* **56** (1960) 424.
19. D. C. PREVORSEK and R. H. BUTLER, *Intern. J. Polymeric Materials* **1** (1972) 251.
20. R. M. BARRER and J. PETROPULOS, *Br. J. Appl. Phys.* **12** (1961) 691.
21. J. CRANK and G. S. PARK, "Diffusion in Polymers" (Academic Press, London, 1968) p. 186.
22. J. H. DUSENBURY, C. N. WU and C. J. DANSIZER, *Textile Res. J.* **30** (1960) 277.
23. J. H. WAKELIN, E. T. C. VOONG, D. J. MONTGOMERY and J. H. DUSENBURY, *J. Appl. Phys.* **26** (1955) 786.
24. G. E. R. LAMB and D. C. PREVORSEK, unpublished data.
25. K. H. MEYER and W. LOTMAR, *Helv. Chim. Acta* **19** (1936) 68.
26. W. J. LYONS, *J. Appl. Phys.* **29** (1958) 1429.
27. L. R. G. TRELOAR, *Polymer* **1** (1960) 95, 279.
28. M. A. JASWON, P. P. GILLIS and R. E. MARK, *Proc. Roy. Soc.* **A306** (1968) 389.
29. P. P. GILLIS, *J. Polymer Sci. A-2* **7** (1969) 783.
30. M. TAKAYANAGI, K. IMADA and T. KAJIYAMA, *ibid C* **15** (1966) 263.
31. R. S. STEIN and F. H. NORRIS, *ibid* **21** (1956) 381.
32. J. C. HALPIN and S. W. TSAI, "Environmental Factors in Composite Materials Design", AFML TR 67-423.
33. P. J. HARGET, *Norelco Report* **18** (1971) 25.
34. M. A. GEZALOV, V. S. KUKSENKO and A. I. SLUSKER, *Vysokomol. Soldin* **A12** (1970) 1787.

35. W. A. STATTON, J. L. KOENIG and M. HANNON, *J. Appl. Phys.* **41** (1970) 4290.
36. G. E. McGRAW, *J. Polymer Sci. A-2* 8 (1970) 1323.
37. D. C. PREVORSEK, *ibid* **4** (1966) 63.
38. D. C. PREVORSEK and W. J. LYONS, *J. Appl. Phys.* **35** (1964) 3152.
39. D. C. PREVORSEK and Y. D. KWON, *J. Macromol. Sci. -Phys.* **B12(4)** (1976) 473.
40. A. R. SACK, *Proc. Phys. Soc. Lond.* **58** (1946) 728.
41. W. T. KOITER, Problems of Continuum Mechanics, Mushkelishvili Ann. Vol. Soc. Ind., Appl. Mech., 1961, p. 246.
42. M. ICHIKAWA, M. OHASHI and Y. YOKOBORI, Reports of the Research Institute for Strength and Fracture of Materials, Tohoku University, Sendai, Japan, **1** (1) (1965) 1.
43. T. J. WILLMORE, *Quart. J. Mech. Appl. Math.* **2** (1949) 53.
44. T. YOKOBORI, M. OHASHI and M. ICHIKAWA, Reports of the Research Institute for Strength and Fracture of Materials, Tohuku University, Sendai, Japan, **1** (2) (1965) 33.

Received 25 August 1976 and accepted 28 March 1977.